



Design of a Preliminary Family of Airfoils for High Reynolds Number Wind Turbine Applications

Cody Karcher *

California State University—Long Beach, Long Beach, CA, 90840

David Maniaci †, Chris Kelley ‡, Alan Hsieh §, Nathaniel deVelder ¶
Sandia National Laboratory, Albuquerque, New Mexico, 87185

Anurag Gupta ||

National Renewable Energy Laboratory, Golden, Colorado, 80401

For the past 30 years, offshore wind turbines exhibited a continual pattern of growth that is expected to continue as the industry pushes for higher efficiency. Current designs for the next generation of wind turbines are so large that the chordwise Reynolds number of the blades is well beyond the design range of existing open-source airfoil families. This paper presents a preliminary family of new airfoils designed specifically for the needs of these next-generation offshore turbines, ranging from 21% thick to 30% thick with operating Reynolds numbers between 12 million and 18 million. These airfoils are intended to be alternative to the FFA airfoils that are commonly used on reference turbines such as the IEA 15MW and 22MW designs. In this work, airfoil performance metrics and design targets are developed, the design process is outlined, an optimization scheme is presented, and finally the airfoils and their simulated performance are compared to existing baselines. Lift to drag ratios in a clean condition were improved by up to 49.3% from the baseline FFA airfoil, and rough condition lift to drag ratio was improved by up to 9.3%. It is estimated that the cumulative improvements provided by this airfoil family would result in an approximately 1% increase of Annual Expected Power (AEP) for the 22 MW turbine compared to the current baseline.

I. Motivation

Current designs for the next generation of offshore wind turbines are substantially larger than the range where we can trust our ability to model them. Though more efficient, the sheer size of these systems introduce new engineering challenges that must be addressed by the research community. One of the most significant challenges is that existing

* Assistant Professor of Mechanical and Aerospace Engineering, Member of AIAA, cody.karcher@csulb.edu

† Principal Member of Technical Staff, Senior Member of AIAA, dcmania@sandia.gov

‡ Principal Member of Technical Staff

§ Senior Member of Technical Staff

¶ Senior Member of Technical Staff

|| Senior Scientist

open-source airfoils were never intended for the high Reynolds numbers encountered by these next generation systems (Figure 1). This lack of appropriate airfoils currently limits the ability to accurately predict the aerodynamics, loads, and power production for blades on wind turbines with capacities above the 5-10 MW range, which is short of the 12-15 MW range for current offshore turbines and well short of the 22-30+ MW turbines envisioned for next generation designs. To reduce the risk of new offshore wind turbine designs, new experimental datasets from wind tunnel and field testing are needed that include high Reynolds numbers (15-25 million [1]) along with studies of real-world erosion, soiling, and stall effects. At present, experimental methods are the most trusted method for obtaining this type of data, where accuracy is critical to adequately modeling the performance of the realized wind turbine system. A robust set of design tools, computational models, optimization approaches, and a new family of tested reference airfoils are also needed to increase confidence in simulations used to assist in the design of next-generation offshore turbines. The present effort aims to address one of these issues by designing high-Reynolds number (15-20 million) airfoils well suited to very large offshore rotor blades that can be used to support the design of future offshore reference wind turbines to serve as an established baseline for future model validation efforts. The primary goal of this paper is to present the design objectives, process, and resulting preliminary airfoil designs to gather feedback from wind energy experts. Future publications are planned that will document improved designs and provide more details into the exact nature of the design process used for this work.

Two publicly available IEA reference turbines exist for the purpose of benchmarking and tool validation: the IEA 15 MW reference turbine that represents current offshore wind turbines, and the IEA 22 MW reference turbine that represents next generation turbines [2-4]. Both rely on the FFA-W3 family of airfoils [5], but exceed the design Reynolds number of the FFA-W3 family by more than a factor of five. Figure 1 also shows the need for test data, as existing validation data is only available for a small region near the tip of these modern offshore turbines. Our primary purpose is to develop a family of airfoils specifically designed for these high Reynolds number offshore reference turbines, with the long term aspiration of eventually gathering experimental data to be used for industry wide validation.

To ensure that the new airfoil family would address the validation and reference model needs of the wind turbine research and industrial communities, interviews were conducted with more than two dozen experts across a wide range of wind turbine design and manufacturing teams over a period of 18 months. An expert advisory panel of industry, research laboratory, and academic members were also solicited to provide more detailed feedback and advice during the design process. The guidance from these experts was used to develop the initial set of airfoil design requirements and design drivers to start the design process (see Section III).

Though this preliminary airfoil family design targets the IEA 22MW wind turbine [4], it is desired that the family can be used on a range of past reference wind turbines (3-5MW) and for the foreseeable future (30MW+). The largest

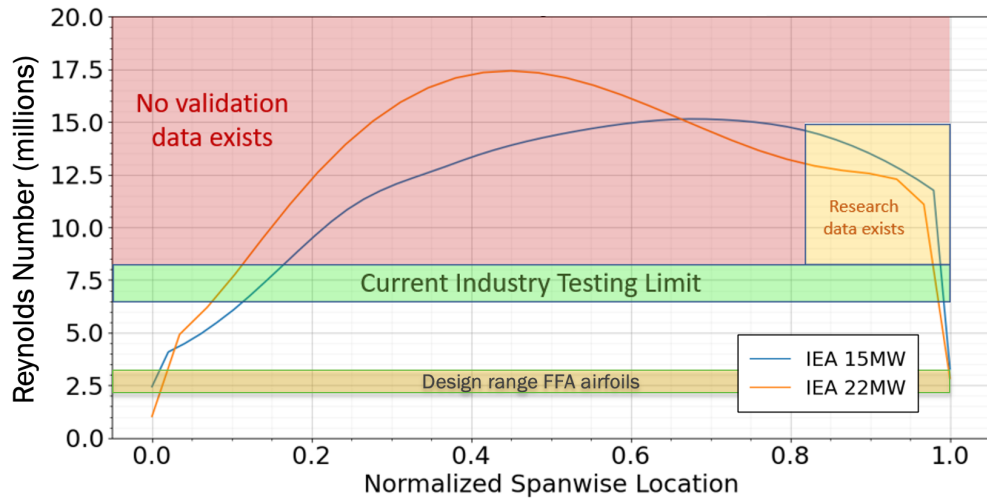


Fig. 1 Existing public airfoils used in reference offshore turbine models (FFA airfoils) are designed for smaller turbines than current state of the art. Current industry airfoil testing does not cover the operating range of modern offshore wind turbines (IEA 15MW) or next generation turbines (IEA 22MW).

envisioned potential future rotor application is a 50MW turbine design that reaches Reynolds number greater than 30 million [6].

II. Design Process

The first step in the design process was to identify key design requirements through consultations with experts in wind turbine design and manufacturing (see Section III). With these requirements and objectives in place, a computational framework was set up to design and analyze airfoils that meet these requirements (Figure 2).

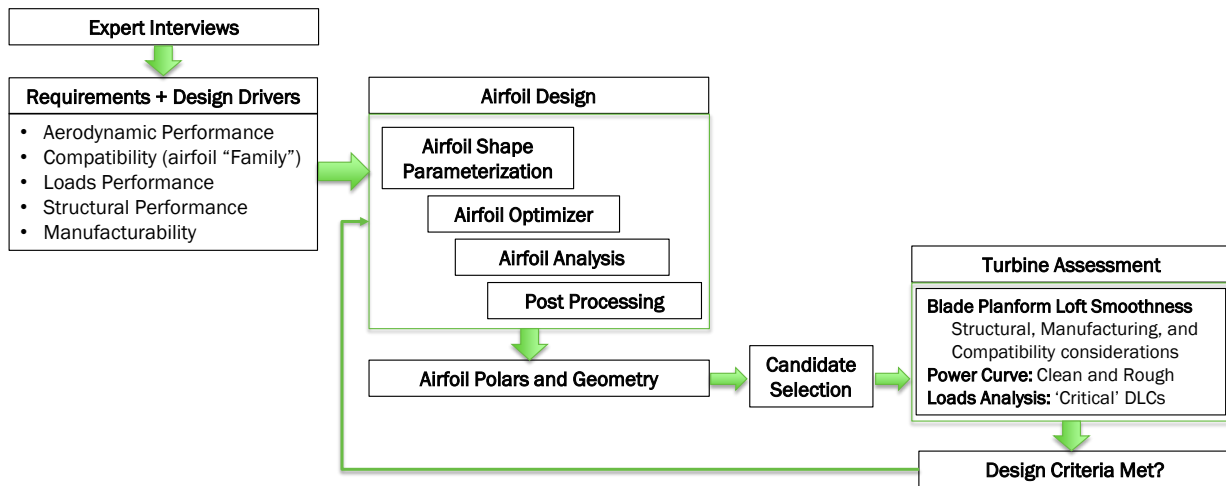


Fig. 2 Airfoil design process flow chart, including requirements definition, design study, and application to target wind turbines.

Despite having several known issues for use in wind turbine design, such as difficulty modeling transition and an over-prediction of maximum lift coefficient, XFOIL [7] was selected as the primary tool for simulating airfoil performance due to its rapid speed and widespread trust throughout the wind turbine and aeronautical communities. Though other tools were considered, no other simulation tool that we or our industrial partners could identify offers the same combination of speed, trust, and computational flexibility on High Performance Computing (HPC) architectures, especially when targeting an open-source design process. In order to get a sense of the error associated with XFOIL, data from the AVATAR project [8] was compared to XFOIL simulations in an effort to establish a qualitative confidence in XFOIL for this application to high Reynolds number turbines (Figures 5 and 6). Though the drag prediction from XFOIL is overly optimistic and the $C_{L_{max}}$ prediction is too high, the primary error in the drag polars is due to an additive shift while the overall shapes of the curves appear visually similar. Seeing this trend, it was determined that XFOIL could be reasonably used for comparing airfoils against each other for the purpose of searching the design space, however absolute predictions of drag coefficient, maximum lift coefficient, lift to drag ration, and similar are not to be taken as ground truth. In this work, we assume that so long as an apples-to-apples comparison is made between airfoils, XFOIL is sufficient to identify designs with high performance potential.

RFOIL [9] is well trusted in the wind turbine community, but is a proprietary code and presently lacks the ability to be run on the Unix-based HPC systems that were used in this design effort. We therefore chose to perform primary analysis using XFOIL, with a final verification in RFOIL to ensure agreement and verify performance. Results from RFOIL do appear in Section VI below. Full Navier-Stokes CFD was not considered as a primary analysis tool due to its computational expense and the lack of calibration or validation data for the desired design space.

Motivated by the AVATAR data, two analysis cases were selected to evaluate airfoil performance that are intended to be representative of two critical stages of the life of a wind turbine in operation. A ‘clean’ case that sets the amplification factor $N_{crit} = 9.0$ and allows for free transition on both upper and lower surfaces and is intended to represent a brand new, idealized turbine. A second ‘rough’ case sets $N_{crit} = 3.0$ and forces transition at 0.05 of normalized chord on both the upper and lower surfaces, which is intended to represent the wind turbine after sustaining the kind of surface roughness typically observed in normal operation. The comparisons between XFOIL and experimental data are presented in the Appendix in Figures 5 and 6 respectively.

Using XFOIL as the core simulation tool, a performance function was written that evaluated and ranked different potential airfoil candidates according to the design metrics discussed below (Section III). This performance function was then driven by a Genetic Algorithm (GA) to produce candidate airfoil designs that perform well with respect to the expert defined requirements list. From this candidate list, we (the authors, in consultation with industry experts) chose the final

airfoil family based on polar, geometry, and additional considerations that were not able to be included in the optimization.

The focus in this work is on the primary outboard airfoil family with airfoils ranging from 21-30% thickness that encompass the outer 40% of the IEA 22 MW blade (shown in 3), as these airfoils are likely to have the most significant influence on the aerodynamic performance of the turbine. The inboard root airfoils (thickness > 30%) used in the IEA 22MW root airfoil section have not been presented here, though airfoils up to 36% thick are under development and airfoils beyond this thickness could be as a part of future work.

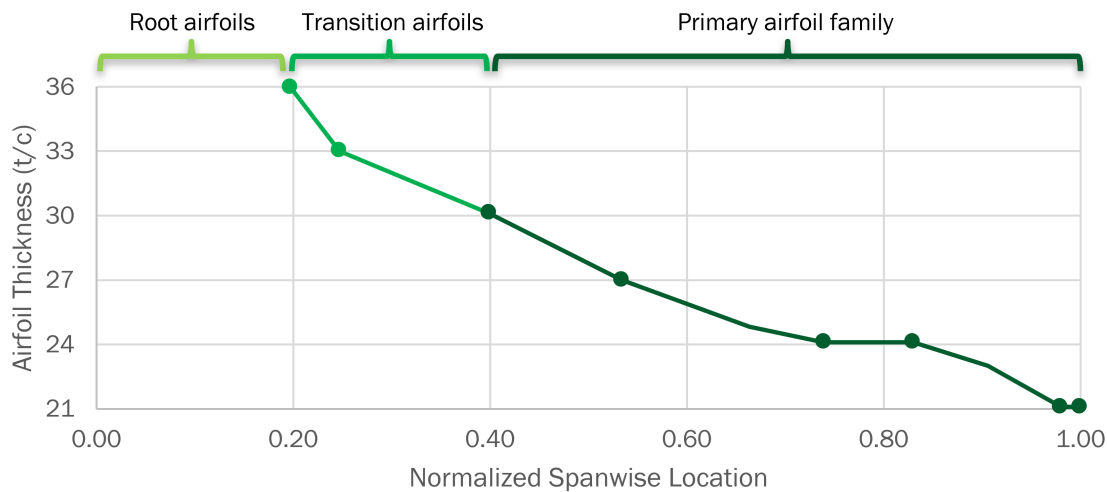


Fig. 3 Airfoil thickness vs. normalized span location for the IEA 22MW offshore reference wind turbine [4]

III. Key Design Drivers

A. Aerodynamic Performance

1. Design Lift Coefficient

Incumbent to the design of any airfoil is the selection of a nominal operating lift coefficient. In the case of wind turbine airfoils, this $C_{L_{\text{design}}}$ should ideally coincide with the maximum Lift-to-Drag Ratio (L/D) of the airfoil. Though selection of $C_{L_{\text{design}}}$ is deeply intertwined with blade design, for this work we simplified this intricate relationship by assuming $C_{L_{\text{design}}}$ is subject to a free design choice. In consultation with industry experts and based on the operating condition of the IEA 22 MW offshore reference wind turbine, we have selected $C_{L_{\text{design}}}$ targets that ranged from 1.5 at the tip of the blade down to 1.2 as mid-span is passed. These design lift coefficients are substantially higher than the design lift coefficients of the other existing airfoils [10–17], which tend to be around 1.0. It is desirable for the design lift coefficient to occur in the linear region of the C_L vs α curve to provide peak efficiency and stall margin. Future work may consider a family of families designed for a variety of $C_{L_{\text{design}}}$ values, or tailored to particular blade design

philosophies, but this was beyond the current scope of work

2. Lift to Drag Ratio (L/D)

Lift to Drag Ratio (L/D) is the primary performance metric for wind turbine airfoils. As a result, our goal was to maximize L/D subject to the key design requirements discussed here. Surveying existing airfoils, the majority come in at a maximum L/D of between 150 and 180, with a notable exception being the Somers S-Series airfoils [14–17]. These airfoils exploit extensive laminar flow on the upper surface to reach higher levels of performance, but exhibited a more limited operating region and a more significant performance degradation at high levels of surface roughness than was ideal for our goals. We therefore focused our efforts on taking a substantial step forward in maximum L/D as compared to the more traditional existing open source airfoil and targeted an L/D for each airfoil in the family that will range from 200 for the thinnest airfoils to 170 for the thicker airfoils. Lift to drag ratio in the rough case was also considered, with targets that ranged between 80 and 110 increasing as we moved outboard. Ultimately, both clean and rough L/D were maximized by the optimizer, however manual modifications were later made to improve rough L/D performance at the cost of clean efficiency.

For the family of airfoils presented here, clean and rough performance were given equal mathematical weight in the optimization. In getting initial feedback from our industry advisors, the general consensus has been that the designs as presented here do not give sufficient weight to the rough (or soiled) case and drive too hard for clean L/D performance, but also noted that soiling concerns decrease in relevance as one moves inboard on the blade. Thus, future work will place more emphasis on the rough flow condition and perhaps introduce a spanwise weighting factor that adds back more clean performance weighting for the thicker airfoils in the family.

3. Stall Margin

Stall margin is critical for ensuring predictable behavior in a variety of real-world conditions. For this work, we defined stall margin as the difference in angle of attack between the where the design lift coefficient is obtained and the angle of attack where peak $C_{L_{\max}}$ is observed, and required a 4 degree margin between these two angles of attack (α_{design} and α_{stall}). For clarity, note that we enforced this as a constraint in XFOIL, which has long, extended stall regions inconsistent with wind tunnel experiments (and also that Tables 2–4 report stall margin from RFOIL simulations). Test data instead reveals stall to occur at a far lower lift coefficient than simulation with a rapid drop off in lift post-stall. At present we, nor our industry advisors, are aware of an openly available simulation tool that reliably captures wind-tunnel behavior, and so XFOIL data was interpreted in light of this known deficiency. RFOIL was used to provide a slightly better prediction of stall behavior as a post-processing step, and somewhat surprisingly had fairly good agreement with the XFOIL data for most of the airfoils proposed here (in contrast with significant disagreements with the FFA and DU airfoils).

In addition to clean stall margin, we also will require the preservation of the same 4 degree stall margin from the angle of attack at the clean $C_{L_{\text{design}}}$ to the angle of attack at the maximum lift coefficient for a rough airfoil. The increase in roughness causes a shift of the stall peak down and to the left on the C_L vs. α curve, and therefore it tends to be the driving stall margin constraint when it is active. Given the limitations of XFOIL, this constraint was rarely observed to be active, though the margin became much tighter in the RFOIL data. The quality of the stall (ie, a sharp peak indicating a rapid drop off vs. a smooth rounded peak of a well behaved stall) tended to be the more relevant design driver, though this was not implemented in the algorithm due to challenges with handling edge cases.

4. Pre-Stall Lift Coefficient Margin

For wind turbines, lift beyond the design lift coefficient is of limited benefit and can become a significant concern in heavy winds. Therefore, though a certain margin above $C_{L_{\text{design}}}$ is required for real-world operation, this margin should be limited. For this work, we define the pre-stall lift coefficient margin to be simply the difference between $C_{L_{\max}}$ and $C_{L_{\text{design}}}$ and have chosen to minimize it with the target goal of a nominally small value of 0.2. However this design target ended up being one of the most difficult ones to meet, as it is in direct conflict with many other valuable design targets, such as rough L/D performance. The preliminary family proposed here effectively sacrifices this criteria in pursuit of other design metrics, however more detailed analysis is needed to determine the impact of this decision. RFOIL data can be used to provide some additional clarity to this design consideration, but the large uncertainty surrounding stall behavior also makes chasing this metric of limited benefit for this work.

5. Change in Lift Coefficient Due to Roughness

The presence of roughness disrupts the boundary layer and causes a decrease in lift which in turn affects turbine efficiency and could limit maximum power production. We define this performance metric to be the change in C_L between clean and rough cases fixed at α_{design} and sought to limit this change to be less than 10%. Though considered and included in the optimization algorithm, this did not seem to be a main driving factor. Maximizing the clean and rough L/D values tended to dominate the affect of this parameter.

6. Change in L/D Over the Airfoil Operating Envelope

In real-world conditions wind turbines do not operate exclusively at the design condition, and so we seek to maximize performance over a wide operating envelope. We defined a performance metric that considered the drop in L/D (in both clean and rough cases) at angles of attack that were 0.85 and 1.15 times α_{design} (eg, $\pm 15\%$ to either side of the design point) and sought to minimize this drop in performance to less than 15%. This assumed range is based on simulations of the IEA 22 MW wind turbine operation with turbulence, and should be sufficient to create a wide operating bucket for

the airfoil and preserve high performance across the majority of the operating envelope. This metric appeared to be one of the most significant, resulting in very large operating ranges that can be clearly seen in Figures 8 through 15 in the Appendix.

B. Structural Considerations

In absence of a coupled aero-structural model, simplified metrics must be imposed on the airfoil design to ensure feasible structural integration. A survey of the existing families of open-source wind turbine airfoils was conducted, and solid area properties were computed for each airfoil. Of the solid area properties considered, the I_{xx} (bending stiffness), I_{yy} (edgewise stiffness), I_{zz} (torsional stiffness), and A (enclosed area) were determined to be well correlated and significantly differentiated from other airfoils that are not intended for wind turbine applications. For each of these four metrics, a locally smooth and monotonic fourth order curve was fit to the lowest value of each metric as a function of airfoil normalized thickness (Figure 7). By implementing these constraints, our goal is to ensure that the structural integration challenge is *no worse* than it is with existing airfoils. These structural constraints should be considered in combination with the geometric constraints covered next section III.C. Figure 7 in the Appendix shows that the limiting case tended to be the RISO-B family of airfoils [12]. The constraints are as follows:

$$I_{xx} = 0.15194621\tau^4 - 0.12744749\tau^3 + 0.05937931\tau^2 - 0.00976398\tau + 0.00059178 \quad (1)$$

$$I_{yy} = 1.36882085\tau^4 - 1.60347502\tau^3 + 0.70416555\tau^2 - 0.11306505\tau + 0.00981479 \quad (2)$$

$$I_{zz} = 1.21138268\tau^4 - 1.41411698\tau^3 + 0.64498366\tau^2 - 0.10370946\tau + 0.00929176 \quad (3)$$

$$A = 19.92943549\tau^4 - 21.37544951\tau^3 + 8.68562194\tau^2 - 1.04486644\tau + 0.1103613 \quad (4)$$

Figure 7 has been included in the Appendix, which shows these constraints plotted along with the relevant data from a variety of open source airfoil families [10–17].

This area of structural considerations has been perhaps the area of sharpest critique when showing the preliminary family of airfoils to industry advisors. The current design process does not include detailed spar layout considerations such as those presented in [4], but issues with inconsistency in the maximum thickness location have caused industry experts to express concern at the feasibility of the proposed designs. Future work will attempt to consider spar layout at a higher fidelity in addition to the simple structural metrics identified here.

C. Geometry Constraints

1. Trailing Edge Thickness

Real turbine blades have non-sharp trailing edges due to practical manufacturing and operation considerations. This is seen in previous work on flatback airfoils [18–20] as well as more recent work for the SUMR 13MW-50MW rotor designs [21, 22]. Our original analysis designed for sharp trailing edges, but this initial family was met with strong resistance from our industry advisory committee. We therefore made a manual modification in the post-optimization process that re-introduced the same trailing edge gaps as the FFA family of airfoils [5]. These thicker trailing edges were particularly beneficial for reducing the drag of higher thickness airfoils in addition to adding structural benefit, and will therefore be adopted in the future as an integrated part of the optimization loop.

2. Leading Edge Radius

Leading edge radius is critical for ensuring acceptable performance across a wide range of angles of attack, and has been suggested as a possible factor in mitigating leading edge erosion. Thus, we sought to preserve a relatively large leading edge radius similar to that of the DU [10] and FFA [5] airfoil families by enforcing a constraint on this value that increases with increasing airfoil thickness. The optimization algorithm was key in identifying high performing airfoils that met this leading edge radius constraint, however the performance metrics were not particularly sensitive to the presence of this constraint in post-optimization trade studies.

3. Trailing Edge Wedge Angle

Practical trailing edges must have sufficient space for manufacturing, and should not hook drastically (ie, a pseudo-Gurney flap should not be allowed). We therefore constrained the final 2% of the airfoil chord to fall outside a 10° wedge drawn from the sharp trailing edge point tangent to the mean camber line at the trailing edge. In practice, this constraint was rarely observed to be a key design limitation, and is likely to require an alternative implementation method in the next design iteration where blunt trailing edges will be included in the core design loop.

4. Maximum Thickness Definition

Airfoil thickness is often defined as taking the maximum y-location on the upper surface and subtracting the minimum y-location for the lower surface. In the majority of cases this definition is adequate, however for some existing airfoil families, these two points occur at notably different values of x/c . A vertical spar cannot be placed between these two points, and so the effective structural thickness of the airfoil is less than the measured thickness. An optimization algorithm will exploit this for improved aerodynamic efficiency but results in unfair comparisons between airfoils that are reportedly of the same thickness. Thus, we enforced that the maximum thickness of an airfoil must be measured perpendicular to the chord line of the airfoil, guaranteeing a spar can be integrated that is of the promised thickness

(however this does not consider twist). The maximum thickness location was also constrained to be aft of the 25% normalized chord location, which was deemed to be an appropriate surrogate for ensuring that the spar could be well positioned down the length of a fully realized blade. As mentioned above, industry feedback has questioned this assumption, and we will look to identify a more robust method of including spar design in the design process moving forward.

D. Additional Considerations

Conversations with industry advisors yielded a few other considerations, and though these did not rise to the level of formal design constraints or objectives, they were considered when selecting final airfoil designs.

- **Aerodynamic Consistency**—Some of the members from our industry advisory committee recommended that we consider the performance of the airfoils as an entire family, with particular focus on aerodynamic similarity. For example, critical angle of attack should be reasonably consistent across the family as to avoid unpredictable or undesirable stall regions across the blade. Similarly, operating angles of attack should be matched to some degree to avoid undesirable twist profiles. At the extreme level, boundary layer parameters, such as shape parameter or wall shear stress, could be matched for similarity to prevent unusual 3D effects. These concerns are somewhat mitigated by the sheer span of the blade, with significant radial distances between airfoil stations. However, this remains of interest for future iterations and likely can be included in a future design iteration.
- **Dynamic Stall Response**—Dynamic stall is not included in the core design process, but will be evaluated in the future using the IEA 22 MW turbine model.
- **Aerodynamic Pitching Moment**—Industry experts were mixed on the importance of pitching moment C_m on airfoil design for wind turbine applications. Some experts identified it as a key parameter, but the narrow majority opined that airfoil pitching moment could be factored out during the blade design using chordwise offsets. Therefore, we tracked this metric and ensured it did not deviate significantly from the baseline FFA airfoil family, but it was not used as a key driver in the design process.
- **Post Stall Behavior**—Post-stall behavior (both positive and negative) is a key factor in blade fatigue, as aero-elastic oscillations can worsen or increase in magnitude with a rapid drop off of lift post stall. Given the limitations of available analysis tools and the inherent lack of trust at predicting post stall behavior, this criteria was not considered in the design loop. It was evaluated to the extent possible by post-process inspection, however the discrepancy between the AVATAR data and simulation, along with the advice of our industry experts, indicates that this design consideration would be more appropriately measured in testing than in simulation.
- **L/D Change Due to Roughness**—Though not explicitly stated above, there is a general desire to minimize the reduction in L/D that is inherent in soiled or rough operation. We considered this design criteria by simply

optimizing for a weighted sum of both clean and rough performance, but a more refined method, such as a multi-objective optimization algorithm, may be used in future work.

E. Summary of Design Criteria

Table 1 summarizes the final list of design criteria that were used in this work, broken out by airfoil thickness. For reference, Tables 2 and 3 show the performance of the FFA family of airfoils used on the IEA 22MW turbine.

Table 1 The desired design targets and criteria used for this work

Normalized Thickness	21%	24%	27%	30%
Design Lift Coefficient	1.5	1.4	1.3	1.2
Reynolds Number	12e6	13e6	16e6	18e6
Angle of Attack	N/A	N/A	N/A	N/A
Clean L/D	200	190	185	180
Rough L/D	110	110	105	100
Stall Margin (degrees)	4.0	4.0	4.0	4.0
Pre-Stall Lift Coefficient Margin	0.2	0.2	0.2	0.2
Change in C_L due to Roughness	0.15	0.14	0.13	0.12
C_M Clean	N/A	N/A	N/A	N/A
C_M Rough	N/A	N/A	N/A	N/A
LE Radius	0.01	0.025	0.03	0.04
Flap Stiffness (I_{xx})	0.00028	0.00041	0.00058	0.00080
Edge Stiffness (I_{yy})	0.00494	0.00561	0.00633	0.00706
Torsion Stiffness (I_{zz})	0.00522	0.00602	0.00691	0.00786
Area	0.11478	0.13051	0.14661	0.16290

IV. Optimization Approach

A Genetic Algorithm (GA) was implemented to identify potential high performing airfoil design candidates based on the performance criteria laid out in Section III. The optimization algorithm is not the main focus of this paper, as we are presenting preliminary designs for the purpose of gathering feedback from the community. We will therefore not be discussing the optimization implementation in detail here, but forthcoming publication will provide more detail on the exact nature of the optimization algorithm along with a release of the code used to generate the final airfoil designs. Instead, we provide a cursory overview of the most important aspects of the optimization used to produce the preliminary designs proposed here.

To identify potential high performing candidates, the design considerations discussed in the previous section were encoded into an objective function which determines the performance or merit of a potential candidate airfoil design. All design criteria are normalized by their approximate expected value to unity, so that the baseline objective has equal weight from all components. Once normalized, an additional weighting factor is applied based on the qualitative value

Table 2 The performance of the FFA airfoils relative to the desired design targets and criteria as computed using RFOIL. Colors have been assigned as a qualitative measure of concern, with grey indicating that the desired target C_L could not be reached, yellow indicating a slight miss on the order of 10% or less, and orange indicating a significant miss. Entries in the first column indicated with an asterisk are reported from XFOIL, as RFOIL struggled to converge at higher angles of attack.

Normalized Thickness	21%	24%	27%	30%
Operating Lift Coefficient	1.5	1.4	1.3	1.2
Reynolds Number	12e6	13e6	16e6	18e6
Angle of Attack	9.82*	8.71	7.75	5.06
Clean L/D	131.16*	135.83	140.56	139.01
Rough L/D	114.61*	108.08	103.19	87.37
Stall Margin (degrees)	7.18*	4.67	4.65	6.44
Pre-Stall Lift Coefficient Margin	0.31*	0.37	0.48	0.80
Change in C_L due to Roughness	0.02*	0.00	0.01	0.17
C_M Clean	-0.097*	-0.115	-0.121	-0.131
C_M Rough	-0.092*	-0.109	-0.112	-0.123
LE Radius	0.0157	0.0321	0.0437	0.0568
Flap Stiffness (I_{xx})	0.00029	0.00045	0.00065	0.00092
Edge Stiffness (I_{yy})	0.00498	0.00613	0.00704	0.00856
Torsion Stiffness (I_{zz})	0.00528	0.00659	0.00769	0.00947
Area	0.11994	0.14022	0.15836	0.18131

of each design parameter. Constraints are implemented using a penalty function and a large constant K which multiplies any constraint violation. The next most highly weighted parameters are the clean L/D at the design lift coefficient along with the rough L/D at the same value of C_L . To this point, these metrics have been given equal weight. The remaining design considerations provide roughly equal contributions that are roughly an order of magnitude less than the L/D targets.

The GA was used to drive this objective function and identify high performing airfoil design candidates using an implementation similar to that described by Deb [23]. Each airfoil was parameterized using the CST parameterization described by Kulfan [24] with 4 design variables representing both upper and lower surfaces (for a total of 8). The GA was run on High Performance Computing (HPC) resources at Sandia National Laboratories, totaling more than 60000 airfoils analyzed per run of the algorithm, and more than 1 million runs of XFOIL. Upon completion of the algorithm, we selected the highest performing airfoil over the course of the run and began with this as a baseline for manual modifications that have been discussed in various sections above. Eventually our goal is to be able to encode sufficient information to the objective function and GA so that a manual design tweak is not required. However, there is inevitably some knowledge gap between our needs and desires as human designers and what we are able to code into the algorithm. Thus, it made sense at this stage to perform the last few design iterations manually.

Table 3 The performance of the DU airfoils relative to the desired design targets and criteria as computed using RFOIL. Colors have been assigned as a qualitative measure of concern, with grey indicating that the desired target C_L could not be reached, yellow indicating a slight miss on the order of 10% or less, and orange indicating a significant miss.

Normalized Thickness	21%	25%	25%	30%
Operating Lift Coefficient	1.5	1.4	1.3	1.2
Reynolds Number	12e6	13e6	16e6	18e6
Angle of Attack	12.75	8.95	7.93	6.69
Clean L/D	68.64	110.33	113.05	131.12
Rough L/D	None	102.43	101.76	99.15
Stall Margin (degrees)	0.24	3.43	4.43	6.76
Pre-Stall Lift Coefficient Margin	0.01	0.25	0.35	0.56
Change in C_L due to Roughness	None	0.04	0.05	0.109
C_M Clean	-0.066	-0.143	-0.146	-0.149
C_M Rough	None	-0.136	-0.138	-0.137
LE Radius	0.01286	0.02578	0.02578	0.03456
Flap Stiffness (I_{xx})	0.00030	0.00052	0.00052	0.00086
Edge Stiffness (I_{yy})	0.00561	0.00654	0.00654	0.00828
Torsion Stiffness (I_{zz})	0.00591	0.00706	0.00706	0.00914
Area	0.12529	0.14818	0.14818	0.17633

In these manual iterations, we prioritized the Additional Considerations that were mentioned in a previous section but not included in the objective function. Aft camber was generally removed to improve structural performance on the back side of the airfoil, and the upper surfaces behind maximum thickness were straightened to improve manfacturability and reduce the risk of buckling. Rough L/D performance was also improved wherever possible. All of these changes came at the cost of clean L/D at the design lift coefficient, but resulted in airfoils that were more reflective of the desires expressed by multi-disciplinary experts and by the industry advisory committee.

V. The Preliminary Airfoil Family

Figure 4 presents our preliminary airfoil family, which ranges from 21% to 30% thick. In general, the family shows a bias towards placing more of the airfoil's enclosed area above the chord line, which we believe is due to the higher operating lift coefficient of this family as compared to the baseline FFAs. However, it has been suggested by our industry advisory committee that this may be the result of sacrificing soiled or rough performance in favor of clean L/D, and so this will be evaluated for future designs.

The 21% thick airfoil had a particularly high lift coefficient target of 1.5, which proved challenging to achieve with high lift to drag ratio. Though the GA was able to meet the performance targets, that airfoil exhibited a rapid onset of stall that was undesirable. Thus, the design reported here has been manually modified to sacrifice clean L/D performance to

obtain more gentle predicted stall behavior. The 21% thick airfoil in particular appears to be in something of a design corner that is strongly boxed off by our design criteria, and proved to be a significant design challenge.

Medium thickness airfoils (24% and 27%) were among the best performing airfoils in the family and met nearly all of their design targets. The shapes show an upward shift of the enclosed area above the chord line, along with reduced trailing edge camber that was intentionally flattened for structural efficiency.

The thicker 30% airfoil is perhaps the worst performer in the family, notably missing both of its L/D targets. Industry experts have suggested this is likely the result of not including blunt trailing edges in the original core design process, and we expect to see significant improvement in future iterations.

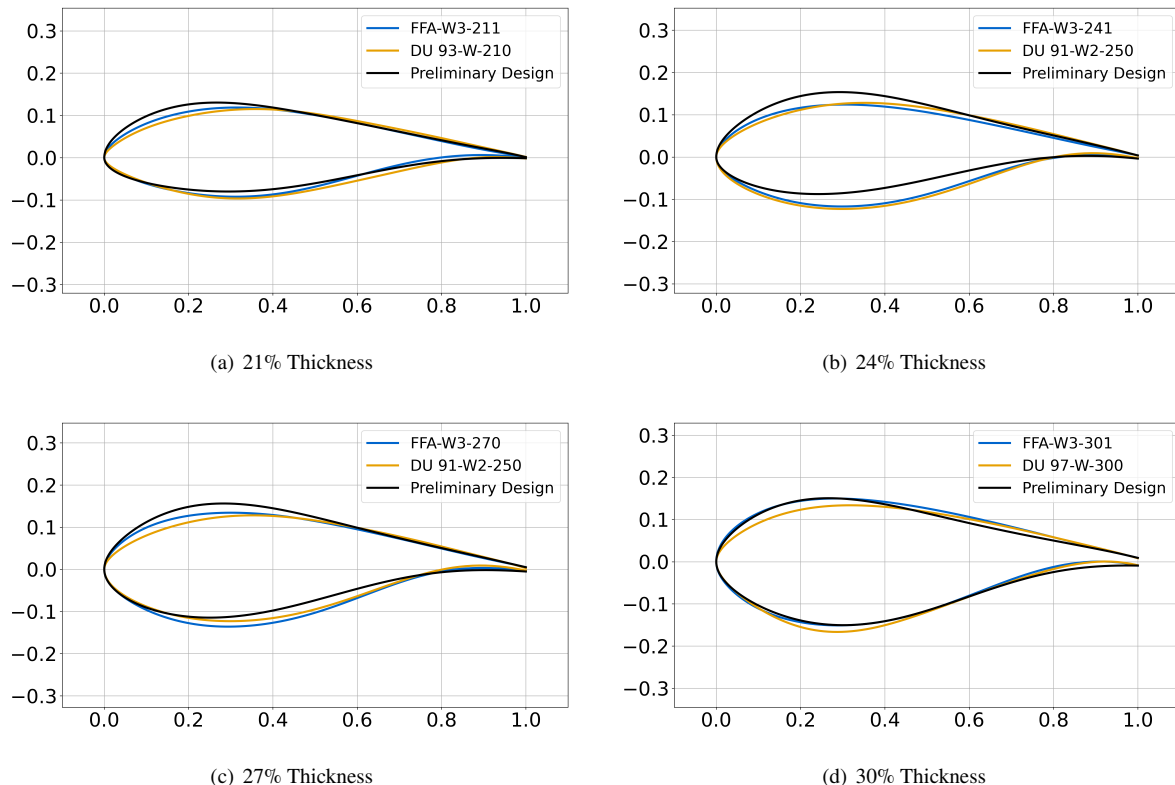


Fig. 4 The proposed airfoil family, plotted with the corresponding FFA airfoils for visual comparison

VI. Airfoil Simulation Results and Performance

Table 4 presents the top-sheet performance of the preliminary airfoil family. On the whole, the preliminary airfoil family performs quite well with respect to the outlined performance metrics, and for the most part out-performs the baseline FFA (and DU) airfoils, particularly with regards to clean L/D performance.

Table 4 The performance of the preliminary airfoil designs relative to the desired design targets and criteria as computed using RFOIL. Colors have been assigned as a qualitative measure of concern, with grey indicating that the desired target C_L could not be reached, yellow indicating a slight miss on the order of 10% or less, and orange indicating a significant miss.

Normalized Thickness	21%	24%	27%	30%
Design Lift Coefficient	1.5	1.4	1.3	1.2
Reynolds Number	12e6	13e6	16e6	18e6
Angle of Attack	9.67	6.39	6.43	7.72
Clean L/D	183.36	202.80	184.58	156.10
Rough L/D	124.14	106.43	109.60	95.42
Stall Margin (degrees)	3.80	4.09	5.98	5.66
Pre-Stall Lift Coefficient Margin	0.39	0.62	0.75	0.81
Change in C_L due to Roughness	0.01	0.08	0.06	0.01
C_M Clean	-0.081	-0.131	-0.118	-0.087
C_M Rough	-0.073	-0.123	-0.110	-0.078
LE Radius	0.02216	0.02881	0.04809	0.05086
Flap Stiffness (I_{xx})	0.00030	0.00043	0.00060	0.00085
Edge Stiffness (I_{yy})	0.00578	0.00637	0.00721	0.00867
Torsion Stiffness (I_{zz})	0.00608	0.00680	0.00782	0.00952
Area	0.12399	0.13782	0.15487	0.17749

Each airfoil was further simulated using both XFOIL [7] and RFOIL [9] at the appropriate Reynolds Number shown in Figure 1 corresponding to the IEA 22MW turbine, and these results are provided in full in the attached Appendix. A comparison to the FFA and DU airfoils is also provided for reference.

The preliminary airfoil family was compared to the following published airfoils: DU [10], RISO-A [11], RISO-B [12], RISO-P [13], S818, S830, S831, S832 [14, 15], and S814, S815, S825, S826 [16, 17]. The preliminary designs presented here outperformed the majority of these airfoils in nearly all performance metrics, however this data has been omitted for visual clarity on the plots and for writing concision. These airfoils have been published in the literature and can be readily compared to the data provided here for any reader who may wish to perform a more detailed comparison beyond the FFA and DU benchmarks provided in the Appendix.

VII. Summary and Conclusions

We have presented a preliminary family of airfoils designed for use in next-generation offshore wind turbines. XFOIL and RFOIL simulation data indicate that these airfoils significantly outperform existing open source airfoils with regards to clean lift-to-drag ratio performance at our desired target Reynolds number and lift coefficient, and outperform most existing airfoils in a rough or soiled state. While not the primary focus of this new airfoil family, the increased L/D of

the new airfoils as presented here is estimated to increase Annual Expected Power (AEP) by 1% for the IEA 22 MW wind turbine with a mean wind speed of 8 m/s.

These preliminary airfoils have been published in order to gather feedback and critique from the wind energy community, with the goal of producing an updated family that will incorporate this feedback into the designs. We the authors welcome input and would encourage those interested to reach out to authors C. Karcher and D. Maniaci to provide feedback and critique for future design iterations.

Appendix

This Appendix contains relevant plots that have been excluded from the main text for reasons of formatting or narrative clarity. The following plots are included:

- Figures 5 and 6 show the comparison between the AVATAR test data [8] and XFOIL [7] predictions
- Figure 7 shows the 2D area properties that were used as structural surrogate models
- Figures 8 through 15 are a full reporting of the analysis data generated by XFOIL and RFOIL for the preliminary airfoil family, along with the simulated results of the corresponding FFA and DU airfoils to provide a point of comparison

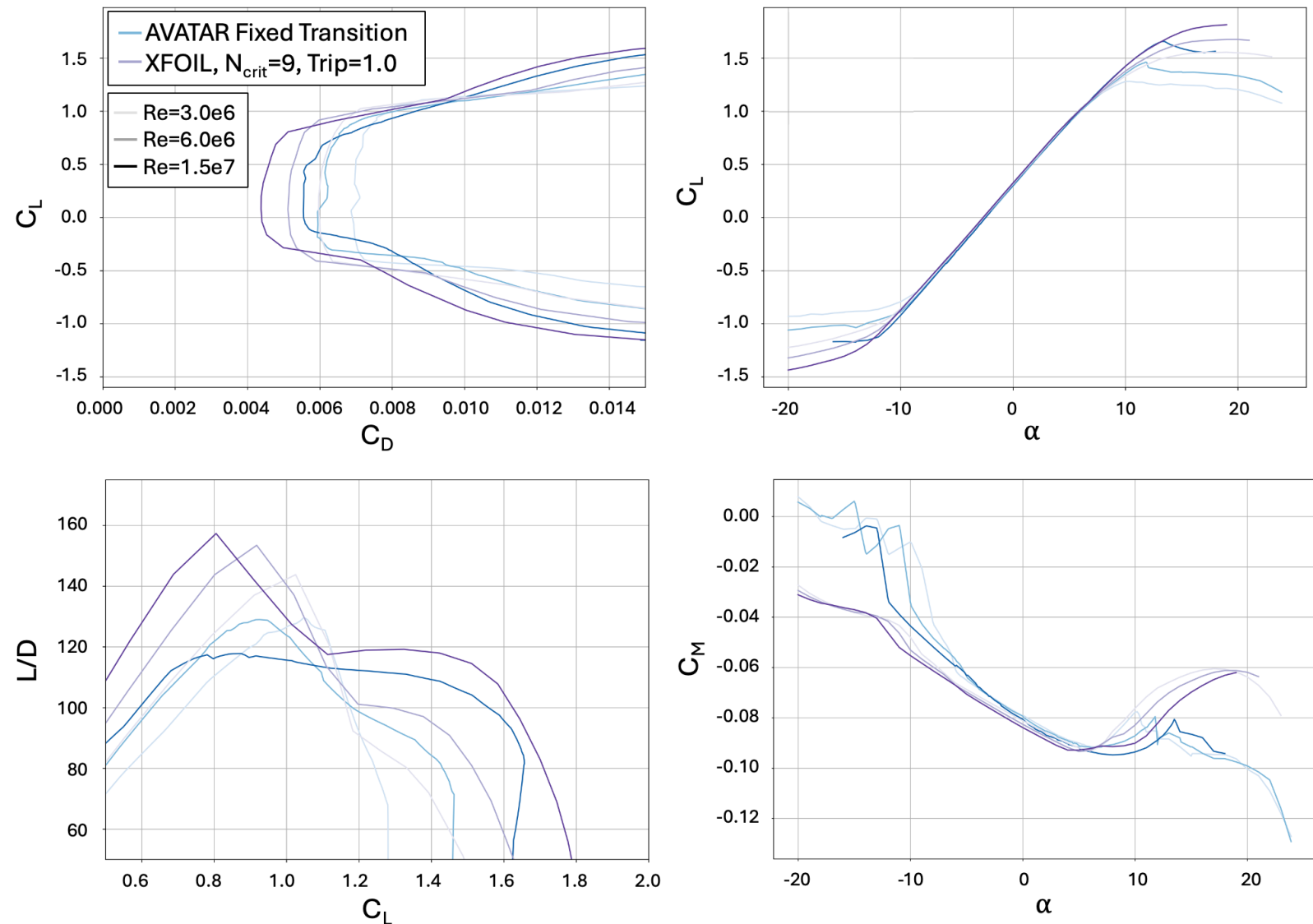


Fig. 5 A comparison of the clean AVATAR experimental data [8] and XFOIL simulation for the DU-00-w-212 airfoil

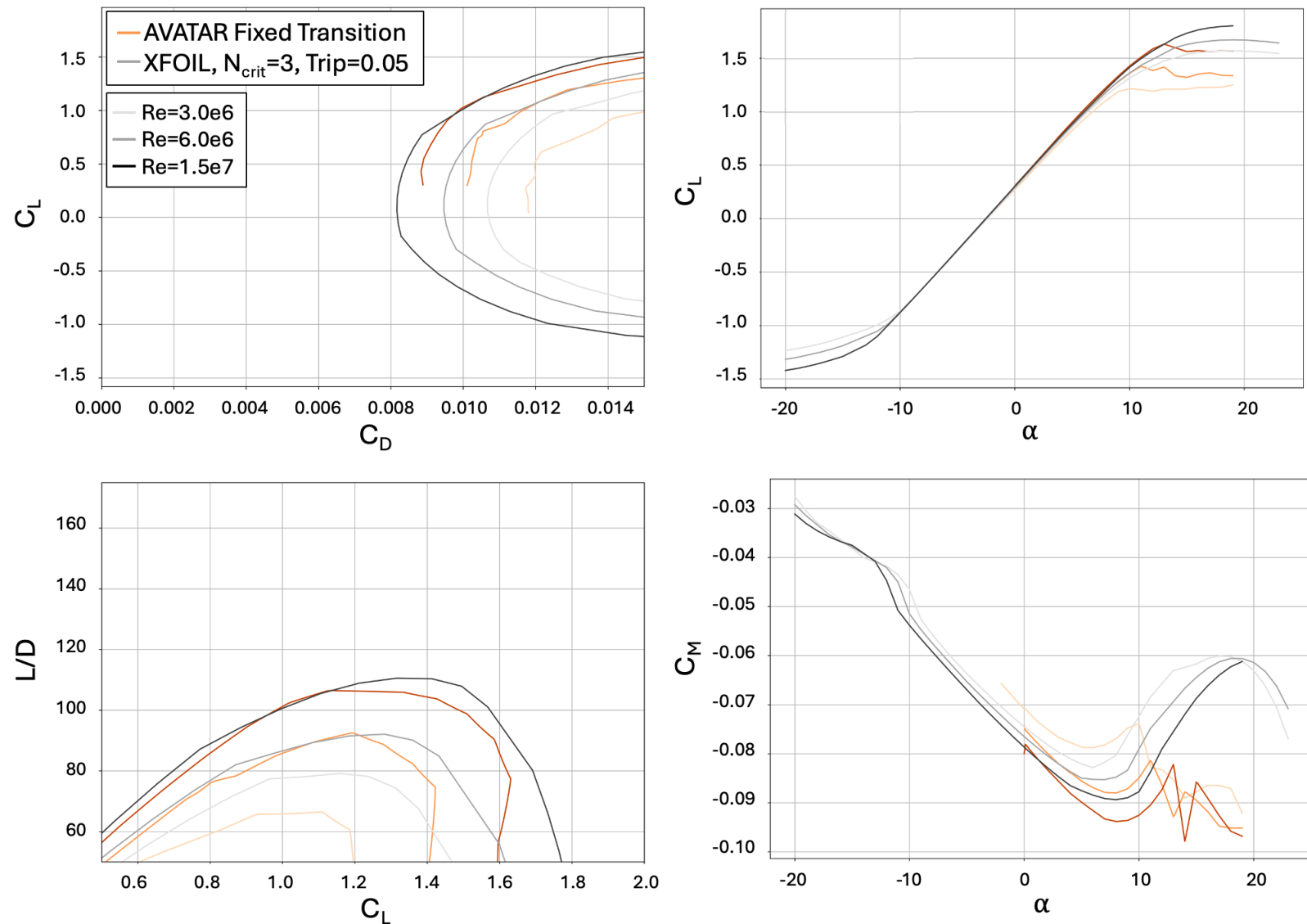


Fig. 6 A comparison of the tripped AVATAR experimental data [8] and XFOIL simulation for the DU-00-w-212 airfoil

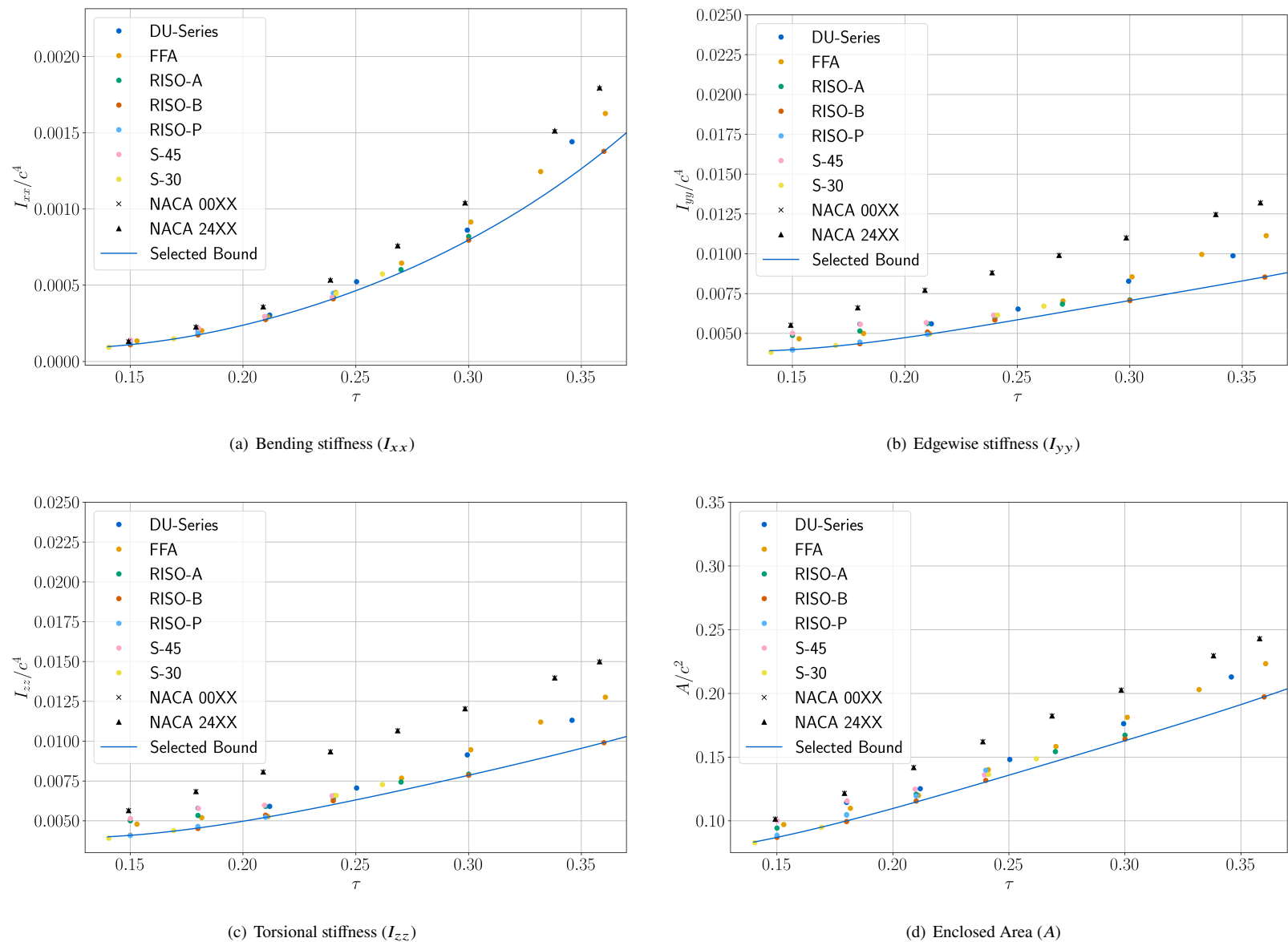


Fig. 7 The solid area properties for existing open-source airfoils, along with the chosen bounds for each property that will be enforced as a surrogate for structural considerations

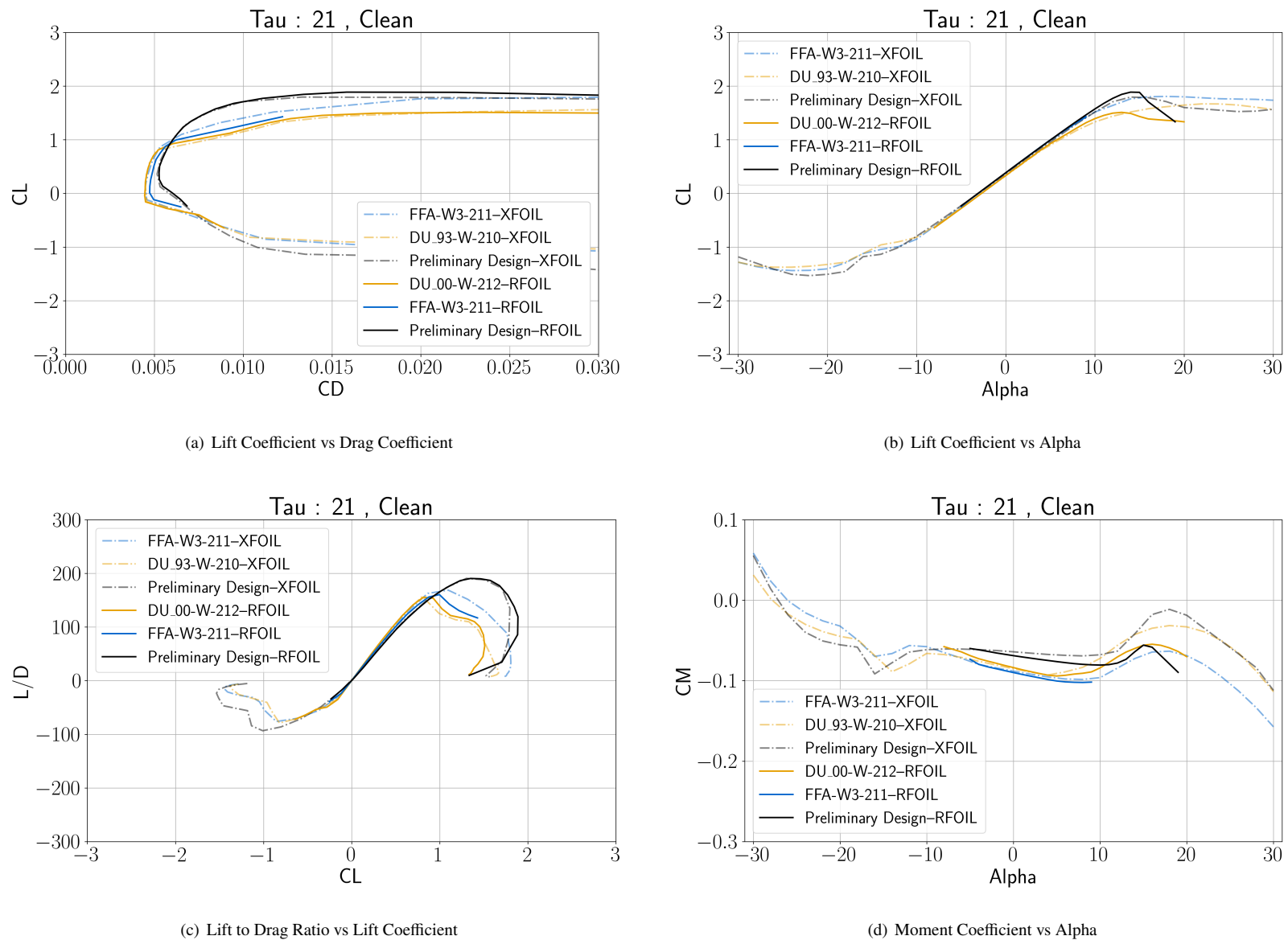


Fig. 8 Analysis Results for the 21% thick airfoil simulating a clean flow condition at a Reynolds number of 12 million

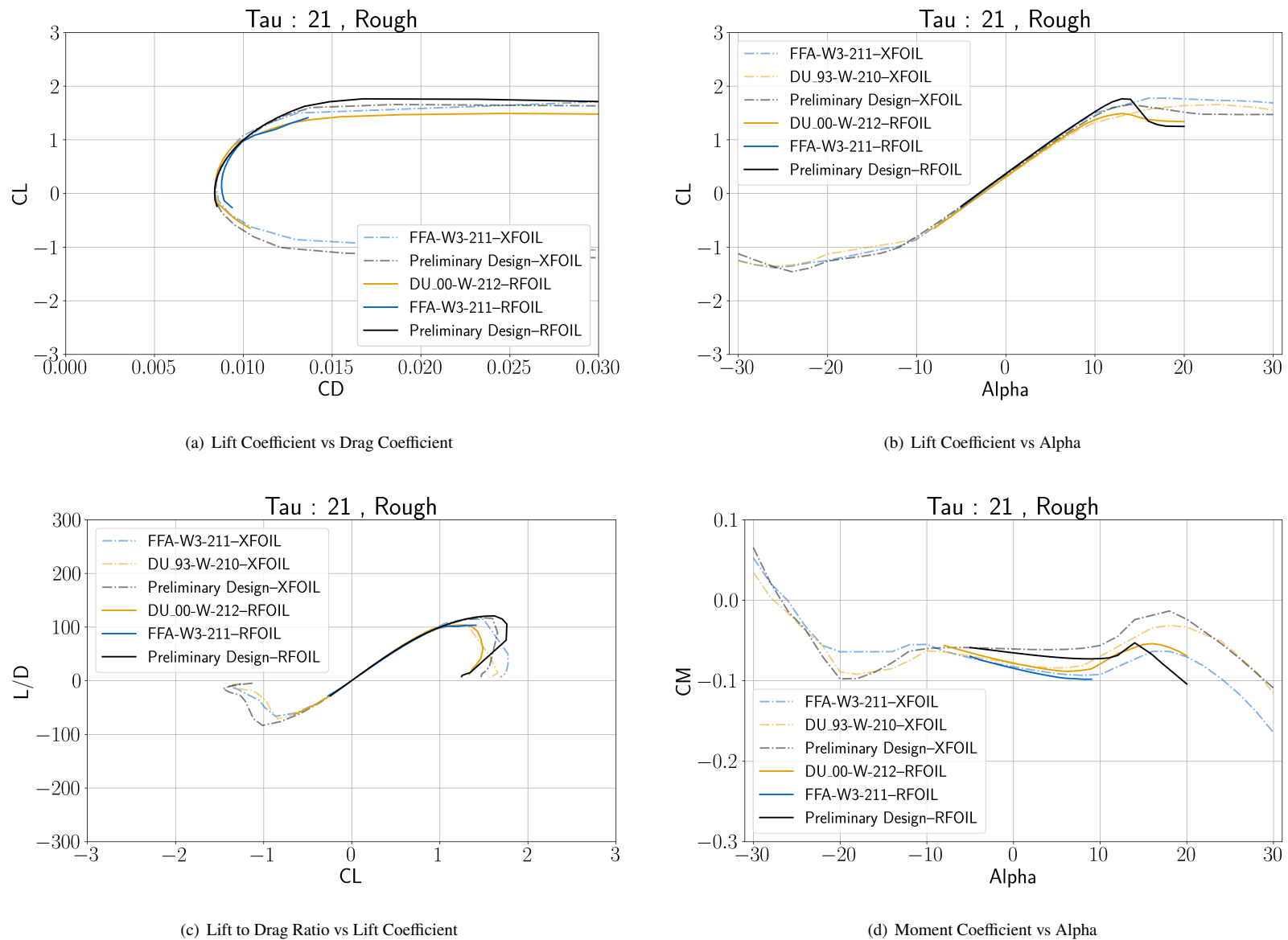


Fig. 9 Analysis Results for the 21% thick airfoil simulating a rough flow condition at a Reynolds number of 12 million

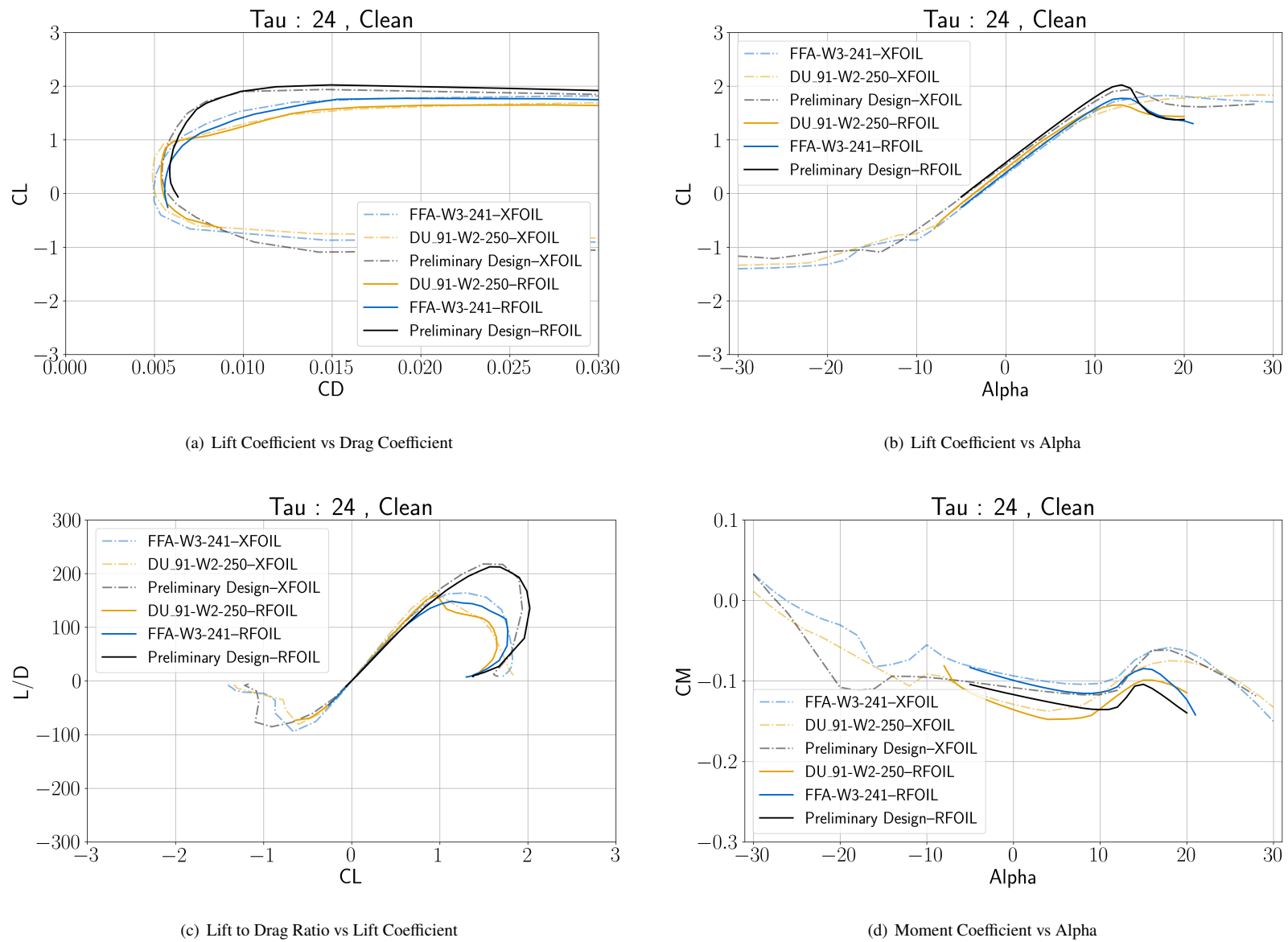


Fig. 10 Analysis Results for the 24% thick airfoil simulating a clean flow condition at a Reynolds number of 13 million

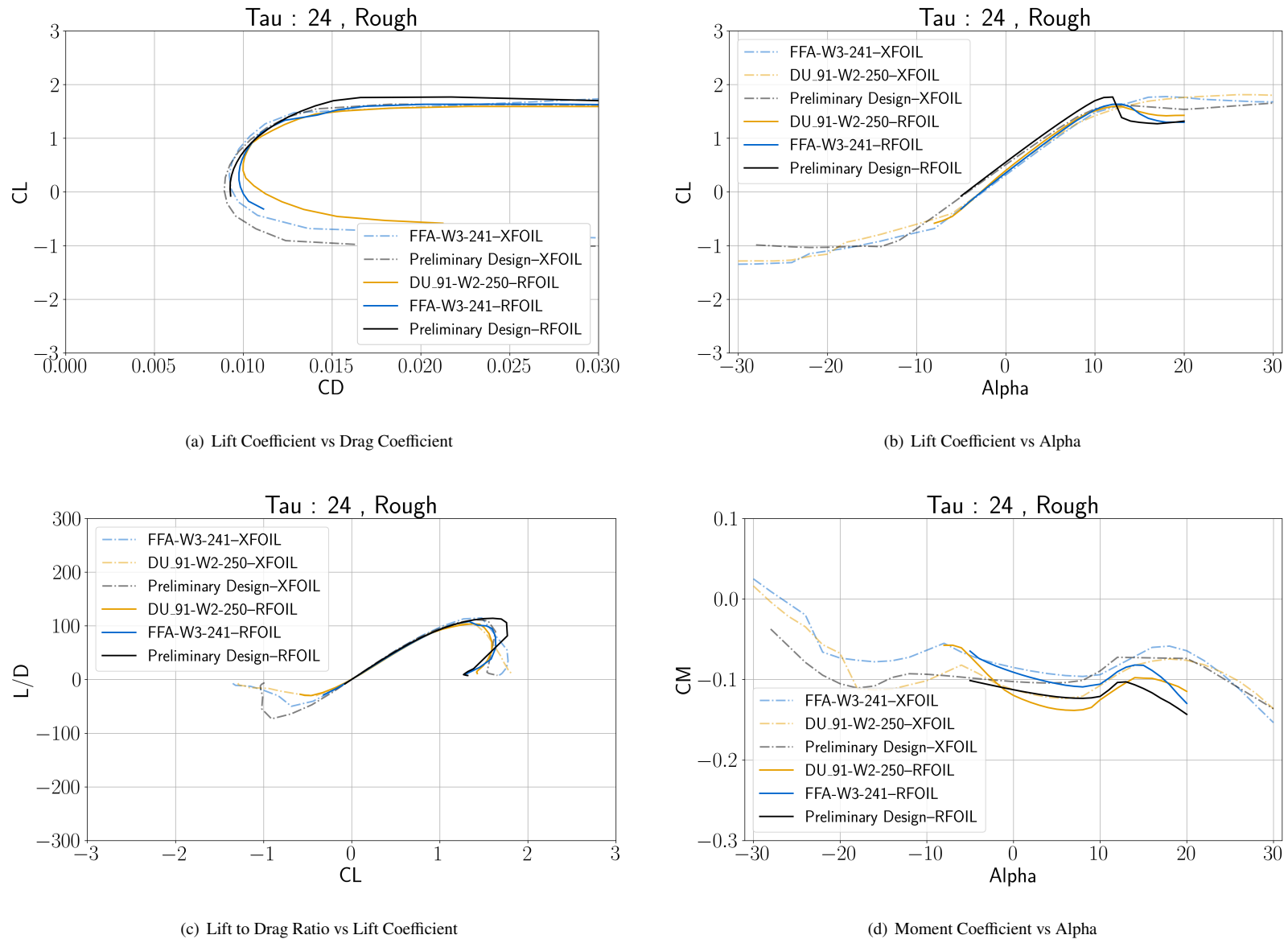


Fig. 11 Analysis Results for the 24% thick airfoil simulating a rough flow condition at a Reynolds number of 13 million

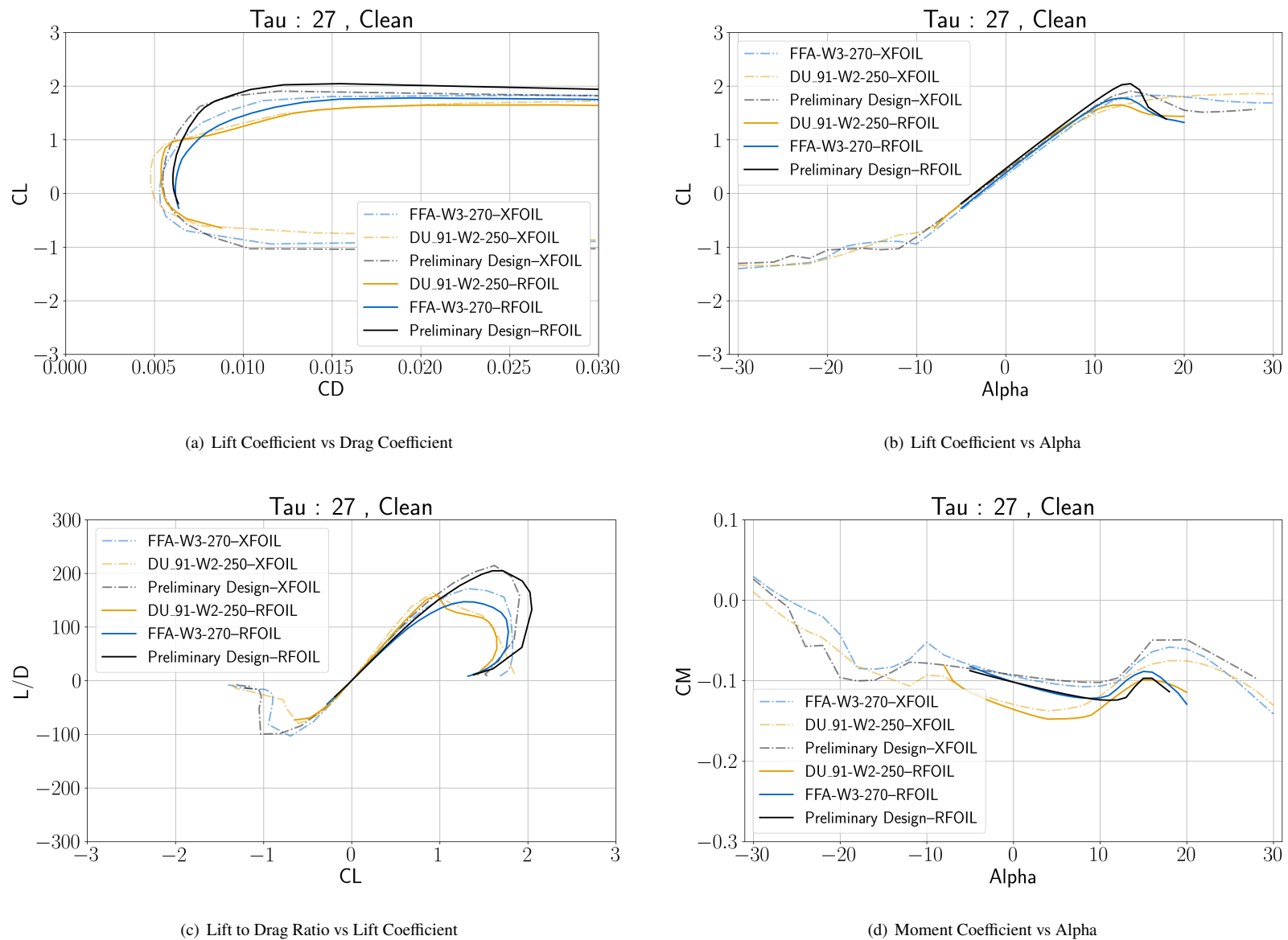


Fig. 12 Analysis Results for the 27% thick airfoil simulating a clean flow condition at a Reynolds number of 16 million

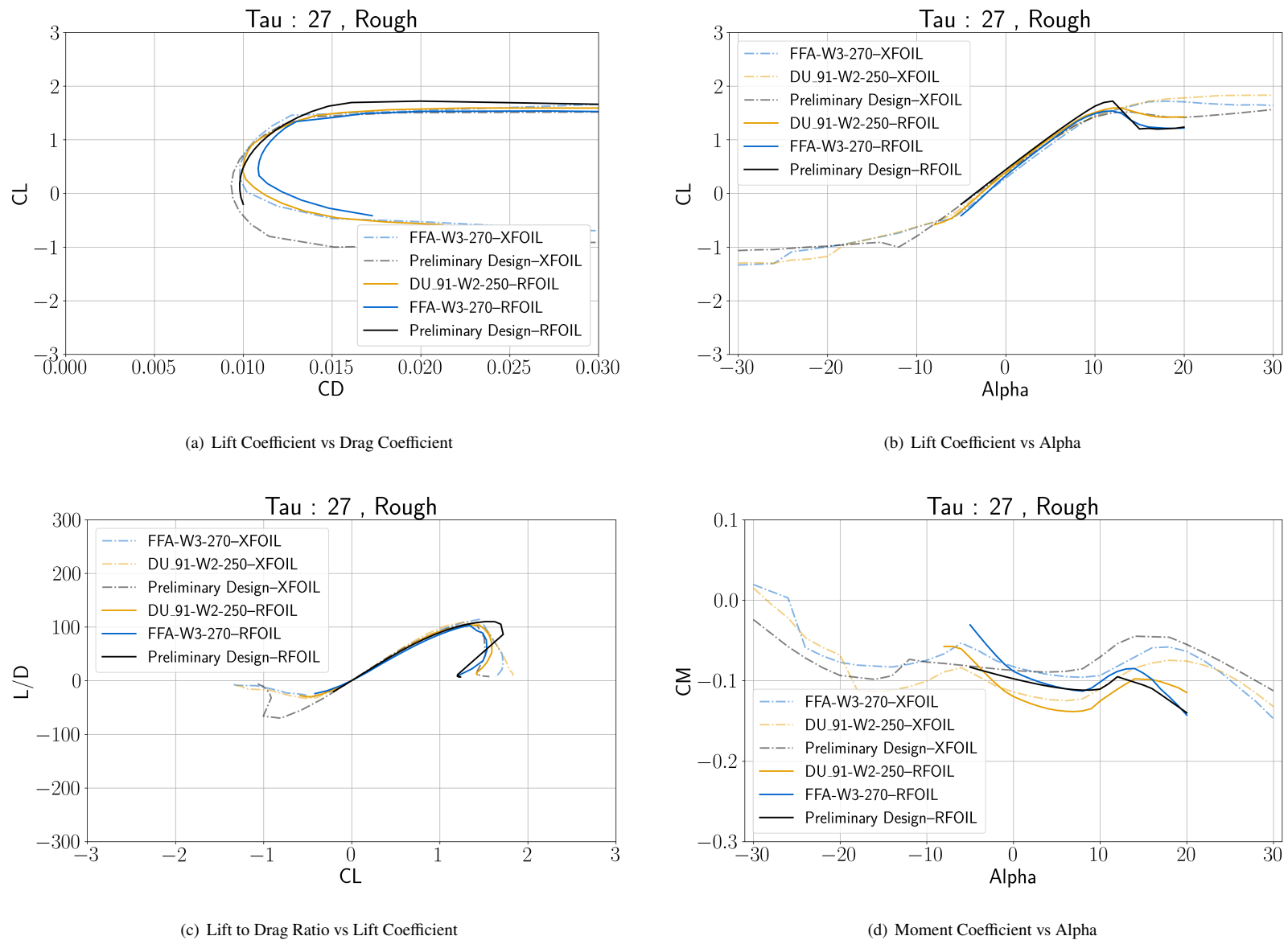


Fig. 13 Analysis Results for the 27% thick airfoil simulating a rough flow condition at a Reynolds number of 16 million

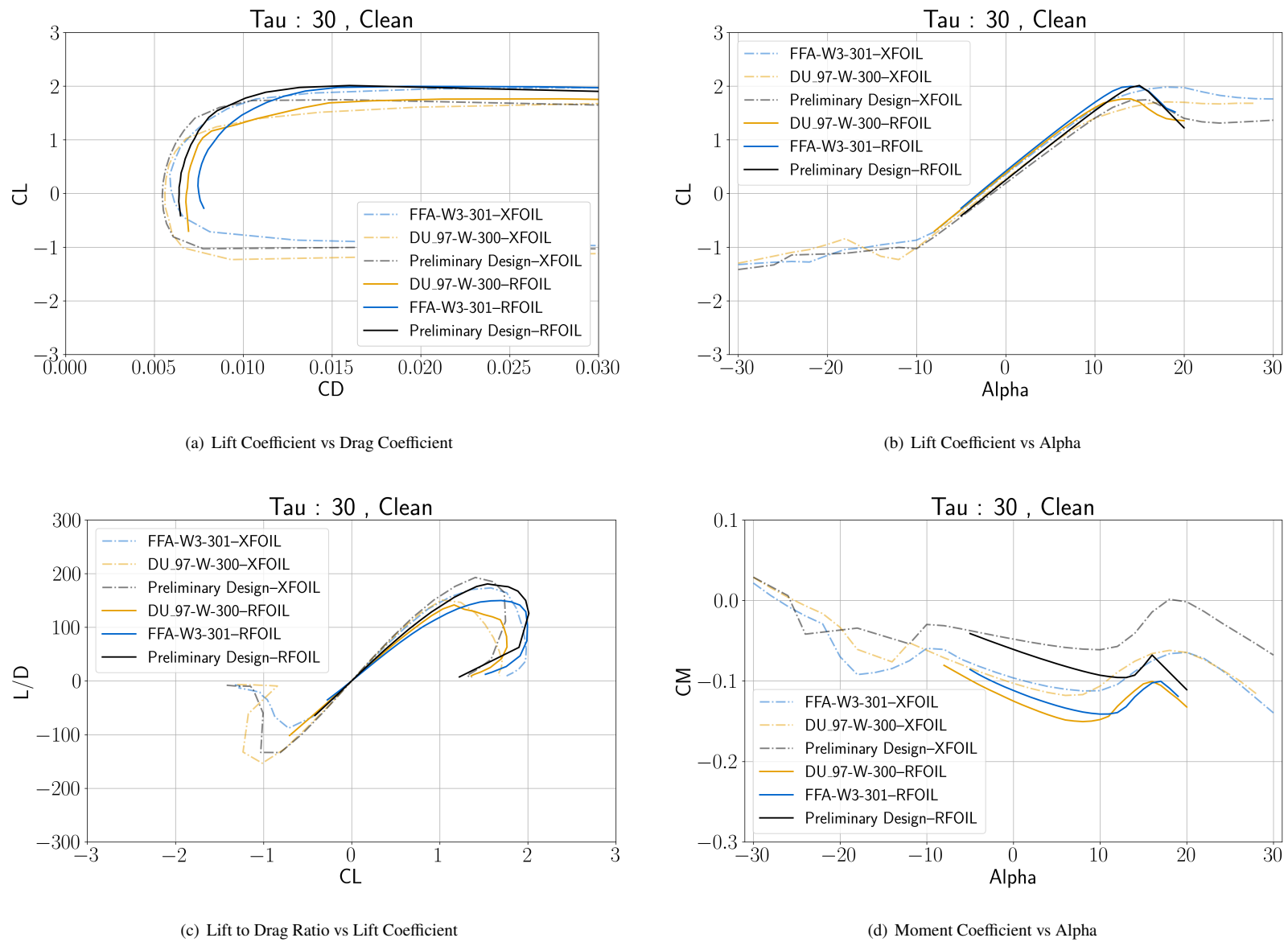


Fig. 14 Analysis Results for the 30% thick airfoil simulating a clean flow condition at a Reynolds number of 18 million

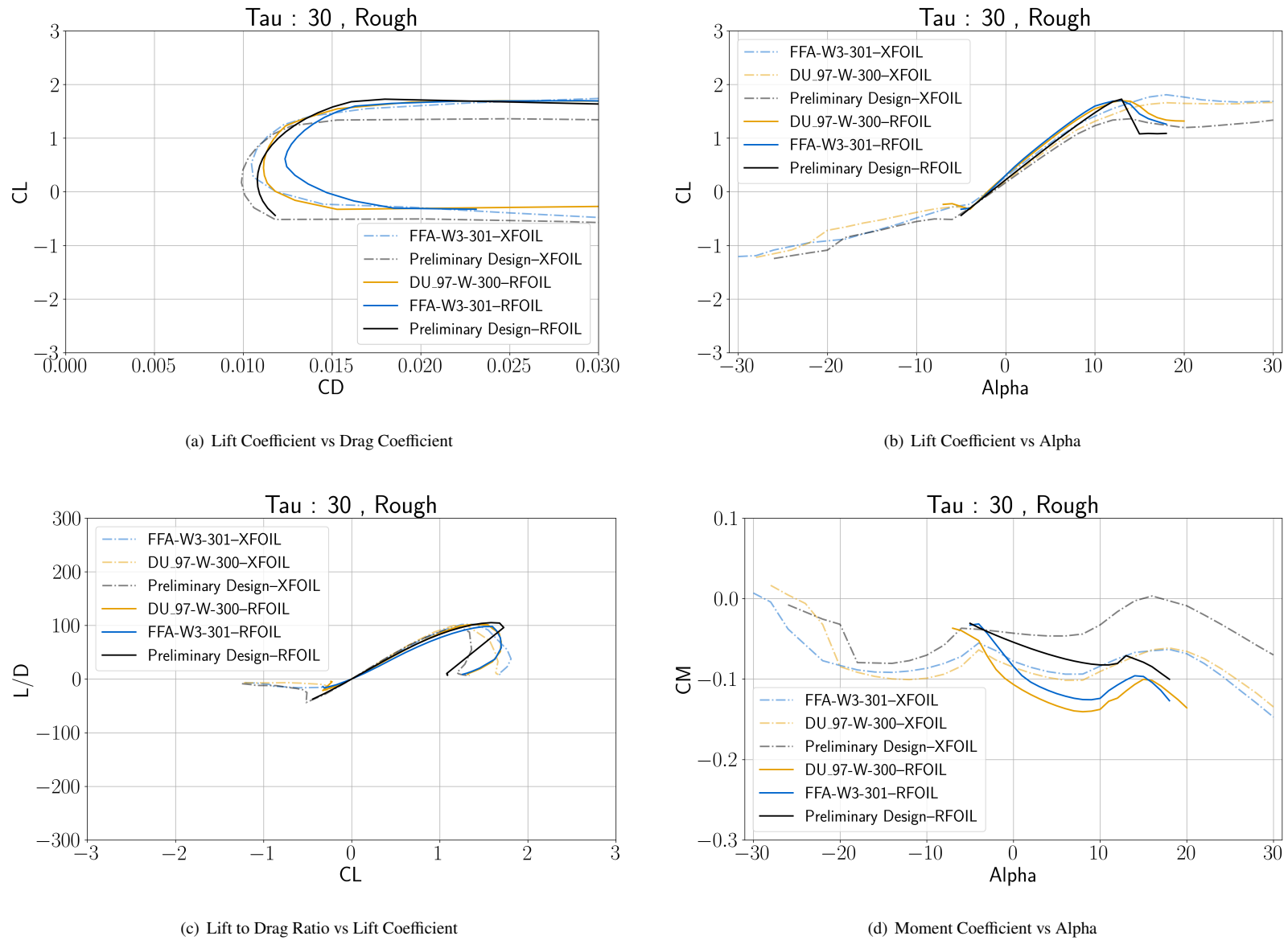


Fig. 15 Analysis Results for the 30% thick airfoil simulating a rough flow condition at a Reynolds number of 18 million

Funding Sources

This work was accomplished through funding from the U.S. Department of Energy Wind Energy Technologies Office. Author C. Karcher is also supported by startup funding provided by the State of California as a new faculty member at California State University, Long Beach.

Acknowledgments

We would like to thank our Industry Advisory Committee for their input and the numerous members of the wind energy community who provided feedback the initial design requirements and these preliminary airfoil designs, and we look forward to their continued feedback and insights.

Sandia National Laboratories is a multimission laboratory managed and operated by National Technology & Engineering Solutions of Sandia, LLC, a wholly owned subsidiary of Honeywell International Inc., for the U.S. Department of Energy's National Nuclear Security Administration under contract DE-NA0003525. The views expressed in the article do not necessarily represent the views of the U.S. Department of Energy or the United States Government. This publication has been assigned number SAND2024-16487C.

This work was authored in part by the National Renewable Energy Laboratory, operated by Alliance for Sustainable Energy, LLC, for the U.S. Department of Energy (DOE) under Contract No. DE-AC36-08GO28308. Funding provided by U.S. Department of Energy Office of Energy Efficiency and Renewable Energy Wind Energy Technologies Office. The views expressed in the article do not necessarily represent the views of the DOE or the U.S. Government. The U.S. Government retains and the publisher, by accepting the article for publication, acknowledges that the U.S. Government retains a nonexclusive, paid-up, irrevocable, worldwide license to publish or reproduce the published form of this work, or allow others to do so, for U.S. Government purposes.

References

- [1] Ceyhan, O., "Towards 20MW Wind Turbine: High Reynolds Number Effects on Rotor Design," 2012. <https://doi.org/10.2514/6.2012-1157>.
- [2] Gaertner, E., Rinker, J., Sethuraman, L., Zahle, F., Anderson, B., Barter, G., Abbas, N., Meng, F., Bortolotti, P., Skrzypinski, W., Scott, G., Feil, R., Bredmose, H., Dykes, K., Sheilds, M., Allen, C., and Viselli, A., "Definition of the IEA 15-Megawatt Offshore Reference Wind Turbine," Tech. rep., International Energy Agency, 2020. URL <https://www.nrel.gov/docs/fy20osti/75698.pdf>.
- [3] Allen, C., Viselli, A., Dagher, H., Goupee, A., Gaertner, E., Abbas, N., Hall, M., and Barter, G., "Definition of the UMaine VolturnUS-S Reference Platform Developed for the IEA Wind 15-Megawatt Offshore Reference Wind Turbine," Tech. rep., International Energy Agency, 2020. URL <https://www.nrel.gov/docs/fy20osti/76773.pdf>.

- [4] Zahle, F., Barlas, A., Loenbaek, K., Bortolotti, P., Zalkind, D., Wang, L., Labuschagne, C., Sethuraman, L., and Barter, G., “Definition of the IEA Wind 22-Megawatt Offshore Reference Wind Turbine,” *Technical University of Denmark*, 2024. <https://doi.org/10.11581/dtu.00000317>.
- [5] Björck, A., “Coordinates and Calculations for the FFA-W1-xxx, FFA-W2-xxx, and FFA-W3-xxx Series of Airfoils for Horizontal Axis Wind Turbines,” Technical Report FFA TN 1990-15, The Aeronautical Research Institute of Sweden, Stockholm, 1990.
- [6] Kianbakht, S., Martin, D., Johnson, K., Zalkind, D., Pao, L., Loth, E., Simpson, J., Yao, S., Chetan, M., and Griffith, D. T., “Design Space Exploration and Decision-making for a Segmented Ultralight Morphing 50-MW Wind Turbine,” *Wind Energy*, Vol. 25, No. 12, 2022, pp. 2016–2035. <https://doi.org/10.1002/we.2781>.
- [7] Drela, M., “XFOIL: An Analysis and Design System for Low Reynolds Number Airfoils,” *Low Reynolds Number Aerodynamics*, edited by T. J. Mueller, Springer Berlin Heidelberg, 1989, pp. 1–12. https://doi.org/10.1007/978-3-642-84010-4_1.
- [8] Pires, O., Munduate, X., Ceyhan, O., Jacobs, M., and Snel, H., “Analysis of High Reynolds Numbers Effects on a Wind Turbine Airfoil Using 2D Wind Tunnel Test Data,” *Journal of Physics: Conference Series*, Vol. 753, No. 2, 2016, p. 022047. <https://doi.org/10.1088/1742-6596/753/2/022047>.
- [9] Van Rooij, R., “Modification of the boundary layer calculation in RFOIL for improved airfoil stall prediction,” 1996.
- [10] Timmer, W. A., and van Rooij, R. P. J. O. M., “Summary of the Delft University Wind Turbine Dedicated Airfoils,” *Journal of Solar Energy Engineering*, Vol. 125, No. 4, 2003, p. 488. <https://doi.org/10.1115/1.1626129>.
- [11] Dahl, K. S., and Fuglsang, P., “Design of the Wind Turbine Airfoil Family RISØ-A-XX,” Technical Report, Riso National Laboratory, Roskilde, Denmark, December 1998. URL https://backend.orbit.dtu.dk/ws/files/7731729/ris_r_1024.pdf.
- [12] Fuglsang, P., Bak, C., Gaunaa, M., and Antoniou, I., “Design and Verification of the Risø-B1 Airfoil Family for Wind Turbines,” *Journal of Solar Energy Engineering*, Vol. 126, No. 4, 2004, p. 1002. <https://doi.org/10.1115/1.1766024>.
- [13] Fuglsang, P., and Bak, C., “Development of the RisøWind Turbine Airfoils,” *Wind Energy*, Vol. 7, No. 2, 2004, pp. 145–162. <https://doi.org/10.1002/we.117>.
- [14] Somers, D. M., “The S816, S817, and S818 Airfoils: October 1991 – July 1992,” Tech. rep., National Renewable Energy Lab (NREL), Golden, CO (United States), 2004. URL <https://www.nrel.gov/docs/fy05osti/36333.pdf>.
- [15] Somers, D. M., “S830, S831, and S832 Airfoils: November 2001-November 2002,” Tech. rep., National Renewable Energy Lab (NREL), Golden, CO (United States), 2005. URL <https://www.nrel.gov/docs/fy05osti/36339.pdf>.
- [16] Somers, D. M., “The S814 and S815 Airfoils: October 1991—July 1992,” Tech. rep., National Renewable Energy Lab (NREL), Golden, CO (United States), 2004. URL <https://www.nrel.gov/docs/fy05osti/36292.pdf>.
- [17] Somers, D. M., “The S825 and S826 Airfoils: Period of Performance: 1994 – 1995,” Tech. rep., National Renewable Energy Lab (NREL), Golden, CO (United States), 2005. URL <https://www.nrel.gov/docs/fy05osti/36344.pdf>.

- [18] Griffith, D., and Richards, P., “The SNL100-03 Blade: Design Studies with Flatback Airfoils for the Sandia 100-Meter Blade.” Technical Report, Sandia National Laboratories (SNL), Albuquerque, NM, and Livermore, CA (United States), September 2014. <https://doi.org/10.2172/1159116>.
- [19] Berry, D., “Blade System Design Studies Phase II : Final Project Report.” Technical Report, Sandia National Laboratories (SNL), Albuquerque, NM, and Livermore, CA (United States), July 2008. <https://doi.org/10.2172/939844>.
- [20] Standish, K. J., and van Dam, C. P., “Aerodynamic Analysis of Blunt Trailing Edge Airfoils,” *Journal of Solar Energy Engineering*, Vol. 125, No. 4, 2003, pp. 479–487. <https://doi.org/10.1115/1.1629103>.
- [21] Ananda, G. K., Bansal, S., and Selig, M. S., “Aerodynamic Design of the 13.2 MW SUMR-13i Wind Turbine Rotor,” *2018 Wind Energy Symposium*, American Institute of Aeronautics and Astronautics, Reston, Virginia, 2018. <https://doi.org/10.2514/6.2018-0994>.
- [22] Jeong, M., Loth, E., Qin, C., Selig, M., and Johnson, N., “Aerodynamic Rotor Design for a 25 MW Offshore Downwind Turbine,” *Applied Energy*, Vol. 353, 2024, p. 122035. <https://doi.org/10.1016/j.apenergy.2023.122035>.
- [23] Deb, K., “Multi-objective optimisation using evolutionary algorithms: an introduction,” *Multi-objective evolutionary optimisation for product design and manufacturing*, Springer, 2011, pp. 3–34.
- [24] Kulfan, B. M., “Universal Parametric Geometry Representation Method,” *Journal of Aircraft*, Vol. 45, No. 1, 2008, pp. 142–158. <https://doi.org/10.2514/1.29958>.